Icarus 250 (2015) 368–383

Contents lists available at ScienceDirect

Icarus

journal homepage: www.elsevier.com/locate/icarus

# Winds, waves and shorelines from ancient martian seas

Don Banfield [a,*], Mark Donelan [b], Luigi Cavaleri [c]

[a] 420 Space Sciences, Cornell University, Ithaca, NY 14853, USA
[b] RSMAS/OS, University of Miami, 4600 Rickenbacker Causeway, Miami, FL 33149, USA
[c] ISMAR-CNR, Arsenale Tesa 104, Castello 2737/F, 30122 Venice, Italy

ARTICLE INFO

*Article history:*
Received 31 October 2013
Revised 26 November 2014
Accepted 1 December 2014
Available online 10 December 2014

*Keywords:*
Aeolian processes
Atmospheres, dynamics
Atmospheres, evolution
Mars, atmosphere
Mars, climate

ABSTRACT

We consider under what environmental conditions water waves (and thus eventually shorelines) should be expected to be produced on hypothetical ancient martian seas and lakes. For winds and atmospheric pressures that are too small, no waves should be expected, and thus no shorelines. If the winds and atmospheric pressure are above some threshold, then waves can be formed, and shorelines are possible. We establish these criteria separating conditions under which waves will or will not form on an ancient martian open body of water. We consider not only atmospheric pressure and wind, but also temperature and salinity, but find these latter effects to be secondary. The normal criterion for the onset of water waves under terrestrial conditions is extended to recognize the greater atmospheric viscous boundary layer depth for low atmospheric pressures. We used terrestrial wave models to predict the wave environment expected for reasonable ranges of atmospheric pressure and wind for end-member cases of ocean salinity. These models were modified only to reflect the different fluids considered at Mars, the different martian surface gravity, and the varying atmospheric pressure, wind and fetch. The models were favorably validated against one another, and also against experiments conducted in a wave tank in a pressure controlled wind tunnel (NASA Ames MARSWIT). We conclude that if wave-cut shorelines can be confirmed on Mars, this can constrain the range of possible atmospheric pressures and wind speeds that could have existed when the open water was present on Mars.



## 1. Introduction

Mariner 9 images first showed geomorphological evidence that water has shaped the martian surface in prominent outflow channels and valley networks, but the final fate of this water has been debated ever since, and is still unresolved. There has been analysis, discussion, and speculation that water responsible for carving channels eventually accumulated, perhaps repeatedly, in relatively large bodies of open or ice-covered water (ponds, lakes, oceans) early in martian geologic history. However, the evidence for standing bodies of water on Mars, whether open or ice-covered, has been circumstantial and controversial. Ocean shoreline morphologies proposed from analysis of Viking Orbiter data were evaluated later with higher resolution Mars Global Surveyor (MGS) imaging and altimetry data, with equivocal results. Smaller bodies of water, especially within large, older impact craters, have also been proposed. The Curiosity Mars Rover was sent to Gale crater, just such an environment, to better understand the geologic history of water on Mars. Not long after landing, it discovered unambiguous evidence of sediments created by flowing surface water (Williams et al., 2013). Determining the fate of flowing water is central to understanding how much water existed, and how long it remained at the surface, with direct implications for the possibility of life developing on the planet. One of the key components of the debate concerning whether water accumulated in standing bodies has been whether ancient shoreline erosion features are still evident. Something that so far has been unrecognized in the debate over these features (or the significance of their absence, in places where other geomorphological evidence is suggestive of standing water) is the following question: Is the expectation of shoreline erosional features a physically reasonable concept?

Terrestrial seas modify their shorelines through the action of wind-driven water waves, as well as tides, tsunamis and the effects of thermal expansion or wind traction on ice sheets. All of these phenomena except tides (because Mars lacks a large moon like Earth's Moon) could also occur on ancient martian seas, creating shorelines. A careful examination of each of these may allow limits to be placed on the ancient martian environmental conditions if evidence of their action can be definitively identified. If no shorelines are ever found, an examination of the ability of various size

* Corresponding author.
*E-mail addresses:* banfield@astro.cornell.edu (D. Banfield), mdonelan@rsmas.miami.edu (M. Donelan), luigi.cavaleri@ismar.cnr.it (L. Cavaleri).

http://dx.doi.org/10.1016/j.icarus.2014.12.001
0019-1035/

shorelines to persist to the present may still allow us to establish limits of the environmental conditions that existed on ancient Mars. The full scope of what can be learned from the current presence or absence of ancient shorelines on Mars is beyond the scope of this work. The magnitude of tsunami waves on ancient Mars was examined by Iijima et al. (2014). Here, we ask under what conditions could wind-driven open-water waves have formed on ancient Mars, leaving the other aspects of the problem to later work.

Evaluating the physics of wind waves in a low-pressure atmosphere affecting a water surface is not a simple exercise of extrapolation from terrestrial experience to very different martian conditions of lower gravity and significantly lower atmospheric pressure. Clearly, reducing the surface pressure to very low values will reduce the capability of the atmosphere to generate waves on a liquid water surface. The pressure at which these atmospheric stresses become insignificant is not yet well understood, but is certainly amenable to investigation. Today, Mars' atmospheric pressure is small (about 0.5% of Earth sea level pressure), but its value in the past is not well constrained. Using models of water waves, we explore the wave conditions that would have occurred on the downwind shores of ancient martian seas subjected to carbon dioxide atmospheres with different surface winds and densities.

Wave formation is fundamental to understanding the potential of shoreline formation. This paper focuses on wave formation under possible conditions on ancient Mars. Section 2 begins by summarizing the present evidence for fossil shorelines on Mars. Section 3 describes wind-wave formation on Earth, the relevant physics of water waves, the two wave-growth models used in this study, and outlines the transition to theoretical martian conditions. Section 4 describes how we validated our generalized wave-growth models against wind-tunnel/wave-tank experimental data under conditions approaching those on Mars. In Section 5, we report the results of the model simulations for a wide range of assumed martian atmospheric and oceanic conditions. Finally, in Section 6, we summarize our results and their implications for constraining conditions on ancient Mars.

## 2. Background – Evidence for fossil shorelines

The notion that Mars once had flowing water on its surface is long-standing, and recent results have strengthened this viewpoint immensely. The earliest evidence to suggest this were the Mariner 9 images of outflow channels with streamlined islands within them and debris aprons at their ends. Using Viking images, Parker et al. (1989, 1993) identified several geomorphologically distinct levels in the northern lowlands, which they proposed were shorelines of an ancient sea. In addition to the proposed shoreline features, Parker et al. also noted that the debris deposits changed character near these same levels at the mouths of the channels, consistent with a change from sub-aerial to sub-aqueous deposition.

The Mars Orbiter Laser Altimeter (MOLA) instrument on MGS provided well-controlled geopotential heights of features on Mars' surface. Head et al. (1998, 1999) and Ivanov and Head (2001) examined Parker et al.'s shoreline features and found that one of their contacts ('contact 2') was at a nearly constant elevation, supporting the argument that it represents an ancient shoreline. They also noted that the circum-Chryse Channel termini all fall within 18 m vertically of one another. However, there were definite differences from an equipotential surface on contact 2, and Parker et al.'s other proposed shorelines were even farther from an equipotential surface. Some of these problems might be explained by tectonic changes since the sea disappeared, isostatic changes from volcanic loading (e.g., Head et al., 1998), the removal of the water itself (Leverington and Ghent, 2004) or true polar wander (Perron et al., 2007).

Malin and Edgett (1999) used MGS Mars Orbiter Camera (MOC) images to examine Parker et al.'s proposed shorelines at higher resolution than was possible with Viking images. They found no evidence to support the hypothesis that ancient shorelines had been preserved, but recognized that identifying shorelines from orbit may be difficult. Carr and Head (2003) synthesized much of the preceding work and concluded that the evidence for Parker et al.'s proposed shorelines was small, but that other lines of evidence strongly support an ancient sea in the northern lowlands of Mars. In particular, the character of the Vastitas Borealis Formation, a veneer covering most of the northern lowlands, is most consistent with sub-aqueous sedimentation of debris transported from the southern highlands to the northern lowlands in the catastrophic floods that carved the outflow channels, and presumably once formed a sea in the northern lowlands.

Most recently, the Spirit and Opportunity rovers identified mineralogy at both landing sites suggesting evaporite minerals. This suggests plentiful ground-water, if not surface waters. Additionally, the hematite-enriched 'blueberries' found at the Opportunity site are believed to be hematite concretions, aided in their formation by significant ground water. The Mars Exploration Rover's (MER's) most compelling evidence is the cross-bedded sediments found in the Eagle and Endurance craters by the Opportunity rover (Squyres et al., 2004). These cross-bedded sediments are most consistent with deposition in a stream-flow environment, i.e., running water at the surface of Mars (Grotzinger et al., 2005). These observations are bolstered by the even more recent discovery by the Curiosity rover of definitive identification of stream-bed deposited gravels (Williams et al., 2013). The evidence for shorelines is still uncertain, with some studies producing no evidence for shorelines (e.g., Ghatan and Zimbelman, 2006), and others finding further evidence of shorelines (e.g., Webb, 2004; Di Achille et al., 2007; de Pablo and Pacifici, 2008; Di Achille et al., 2009; Di Achille and Hynek, 2010; Erkeling et al., 2012). Ghatan and Zimbelman (2006) found no shorelines, but recognize that this could have been due to a lack of waves on an ancient sea. Irwin and Zimbelman (2012) compared terrestrial paleo-shoreline indicators to what we might expect to find at Mars, and concluded that only highly degraded shoreline indicators would be likely to be found on Mars, even if shorelines were once robust. Kraal et al. (2006) argue that ancient lakes would be unlikely to have sufficient time to incise a shoreline into bedrock, even with waves of terrestrial strength, however this only addresses bedrock-incised shorelines, while other landforms could still produce and possibly retain shorelines. Although the debate is still uncertain, it places increasing pressure and interest on resolving the possibilities of standing water at the martian surface in some locations, for some periods of time.

A key unresolved question is how to reconcile the marginal evidence for shorelines with other evidence pointing to a sea in the martian northern plains in the past. The absence of ancient, preserved shorelines may not be evidence that a sea did not once exist on Mars. Rather, if a sea ever did exist, it may be that atmospheric and other environmental conditions might have been unfavorable for creation of prominent, robust shoreline morphologies. These issues also apply to ponds and lakes proposed for smaller basins, e.g., provided by impact craters in the southern highlands. Our target in this paper is to clarify if wind waves are indeed possible in atmospheric conditions substantially different from the ones we are used to on Earth. Principally, the atmospheric pressure is a key variable in influencing the ability of the atmosphere to transfer energy to the sea, which eventually is then deposited on the shoreline. Without this energy transfer, there would be no erosional/depositional shoreline, even in the presence of a sea.

This work addresses wind-wave generation processes in open bodies of water (i.e., not ice-covered). Current conditions on Mars for low-salinity oceans would eventually result in an ice-covered body of water. However, the thermal environment of ancient Mars, as well as the ultimate salinity of ancient martian seas, is unclear (e.g., see Fairen, 2010). Additionally, due to the effectively high thermal inertia of a convecting sea, even if Mars were too cold for stable liquid surfaced seas, it would still take some considerable time for a sea to freeze (Carr, 1996). During this time, if sufficiently large waves can be developed, a shoreline might be formed. For the places on Earth where shorelines annually freeze and thaw, the majority of the shoreline modification often occurs with open water, as forcing by waves can be more efficient than by ice in depositing energy directly on the shoreline (Forbes and Taylor, 1994). Consequently, and due to the unknown climate history of Mars, this work is focused on the ability of winds at various atmospheric pressures to create water waves and presumably thus shorelines.

## 3. Wave modeling

On Earth the physics concerning the generation and development of wind waves is fairly well understood. Present wave models perform in general at a very high level, their operational accuracy for terrestrial applications often being comparable to that of the measuring instruments. In the present work we have used two different, but well established, wave models to simulate the possible wave conditions in the Mars environment. The physics of the models must be adapted to the different possible Mars conditions. However, apart from changing the values of some basic physical variables (e.g., gravitational acceleration, atmospheric and liquid density, atmospheric pressure, and liquid viscosity and surface tension), no ad hoc calibration has been done on the models. Because the wave models are built and expressed in terms of the fundamental physics (as opposed to empirical fits), we have confidence that extrapolating them to the foreign conditions of ancient martian seas is likely to be accurate. However, to validate their accuracy over the large extrapolations required, we have also successfully proven these same models against wind tunnel tests for conditions between terrestrial and (approaching) those on current Mars. Because of this, we have a high degree of confidence in our ability to accurately model wave conditions that could have existed on ancient martian seas.

To further increase our confidence in our modeling of waves under possible ancient martian conditions, we use and inter-compare two modern spectral models of Earth wave growth and propagation: UMWM, developed by Donelan et al. (2012), and SWAN, developed by Booij et al. (1999). If our two independent models can both match our wind tunnel data, as well as one another when extrapolated to realistic ancient martian conditions, we will conclude that their results are accurate. The key aspects of our work in converting these models from terrestrial to martian conditions lie in identifying all of the terms that are likely to be modified in the martian environment, and ensuring that they are explicitly handled in all of the aspects of the models. In the rest of this section, we review water waves, discuss the model parameters that are expected to change on Mars, and finally identify in which terms of the models these modified parameters appear.

### 3.1. Physics of surface water waves

Water waves are oscillatory perturbations to the surface of a liquid. For long wavelength ($\lambda$) waves, the restoring force maintaining the oscillation is gravity. For wavelengths shorter than some cutoff length, surface tension takes over and dominates. On Earth, this cutoff occurs for wavelengths of about 2 cm. On Mars, with a reduced gravity, and perhaps a different surface tension with briny waters, this cutoff may occur at different wavelengths. Because on Earth these cutoff lengths are usually quite small, one usually only thinks of gravity as the restoring force for water waves. However, because the first waves to grow are near this cutoff length, in considering the possible generation in different conditions the effects of surface tension must be taken into account.

The phase speed of a water wave depends on whether it is propagating in water that is deep or shallow compared to its wavelength. Typically, in considering the growth phase of a wave spectrum, the waves are assumed to be in deep water, and only when they move into depths lower than half the wavelength, then approach the beach and start breaking, are they treated as shallow water waves. The relation between the wavelength of the wave and its phase speed is known as the dispersion relation of the waves. For deep-water waves, this can be written as: $c = \sqrt{\frac{g}{k} + \frac{kT}{\rho}}$, where $c$ is the wave's phase speed, $k$ is its wavenumber ($2\pi/\lambda$), $d$ is liquid depth, $g$ is the acceleration of gravity, $\rho$ is the liquid density and $T$ is the surface tension. By deep-water waves, we mean that the product of wavenumber and depth (i.e., $kd$) is large. This means that the water depth is significantly larger than the wavelength of the waves. From the dispersion relation, we can see that long waves on Mars (gravity dominated) will move more slowly than on Earth (for the same wave period) because of the reduced gravity. The separation between gravity-dominated and surface tension dominated (capillary) waves can be seen to be $k_0 = \sqrt{\frac{g\rho}{T}}$. These are also the slowest waves. Thus, a reduction of gravity by a factor of 3 corresponds to a ~73% increase in the wavelength of the capillary-gravity division – still too short to be relevant except in the earliest stages of generation by wind.

While the wave crests move at the phase velocity, a train of waves will propagate at their group velocity, which in the case of long (gravity-dominated), deep-water waves is half the phase speed, $C_g = \frac{g}{2kc} + \frac{3kT}{2\rho c} \approx \frac{c}{2}$ (if $kd$ is large and $k \ll k_0$).

### 3.2. Modeling

Wave conditions at a given time and space are represented by their wave spectrum $F(f,\phi)$ or $F(k,\phi)$, with $f$ the wave frequency related to wavenumber $k$ by the dispersion relationship $\omega^2 = gk\tanh(kd)$ with $\omega = 2\pi f$ and $d$ the local depth. In practice the wave conditions are considered as a superposition of a large ($nf \times n\phi$) number of wave sinusoidal components, each characterized by frequency (hence period and wavelength), direction $\phi$, and energy.

For given wind speed and basin geometry, the evolution in time and space of the wave spectrum is expressed in terms of the radiative transfer equation (written for $F(k,\phi)$)

$$\left(\frac{\partial}{\partial t} + \nabla \bullet C_g\right) F(k,\phi) = S_{\text{in}} + S_{\text{nl}} + S_{\text{diss}} \tag{1}$$

where the left hand side of the equation expresses the conservation of wave energy as the wave field evolves, i.e. propagates, in space and time, while the right hand side consists of the sources and sinks of wave energy. $S_{\text{in}}$ is the energy input from the wind, $S_{\text{nl}}$ represents non-linear wave–wave interactions, $S_{\text{diss}}$ is the energy loss due to various deep and shallow water processes. Indeed $S_{\text{diss}}$ can be split into various components, $S_{\text{diss}} = S_{\text{visc}} + S_{\text{wb}} + S_{\text{bf}} + S_{\text{br}}$, where $S_{\text{visc}}$ is the viscous dissipation, $S_{\text{wb}}$ is breaking (including white-capping and micro-breaking) in deep water, $S_{\text{bf}}$ is the loss due to bottom friction, $S_{\text{br}}$ is the loss due to shallow water wave breaking. See Komen et al. (1994) and Holthuijsen (2007) for a both general and detailed description of Eq. (1) and all its terms.

*3.2.1. The UMWM model*

In the UMWM the source terms of the radiative transfer equation are summarized as $S_{in} + S_{wb} + S_{nl} + S_{bf} + S_{br}$, where $S_{in}$ includes both generation by wind and viscous damping. Observational evidence for $S_{in}$ has accumulated over the past decades and, coupled with the results of numerical modeling, the form and strength of $S_{in}$ can be said to be quite well known. Based on comparison with wavenumber spectra of gravity waves measured in the North Sea, Donelan et al. (2012) find:

$$S_{in} = 0.11\frac{\rho_g}{\rho_l}|U_{\lambda/2}\cos\theta - c - u\cos\phi - v\sin\phi| \times (U_{\lambda/2}\cos\theta - c - u\cos\phi - v\sin\phi)\frac{\omega}{c^2}F(k,\phi) - 4\nu k^2 F(k,\phi) \quad (2)$$

where $\rho_g$ and $\rho_l$ are the overlying gas and liquid density, $U_{\lambda/2}$ is the wind speed at half the wavelength height, $\theta$ is the angle between the wind direction and waves traveling in direction $\phi$, $u$, $v$ are the east and north components of the surface current, $\omega$ is the intrinsic frequency of waves of wavenumber $k$, and $\nu$ is the liquid viscosity. The first term on the right is the wind driven wave growth, while the second term is the wave damping from viscosity (only important for large $k$, i.e. short wavelengths). Careful fetch limited growth studies in the field corroborate this form for $S_{in}$, at least under terrestrial sea-level conditions.

This term represents the only dependence of the problem on gravity or the density of either fluid. As mentioned above, we expect the changes in gravitational acceleration, air density and wind speeds to be the most important differences between Earth and Paleo-Mars, so properly accounting for these effects is critical. While we believe that they are correctly and completely accounted for in our wave evolution models, we describe below (see Section 4) how we have verified the gas density effect by using a pressure regulated wind tunnel.

The second most important change between Earth and ancient Mars is likely to be in the viscosity of the water, as evidence suggests martian sub-aqueous sediments were deposited in highly concentrated brines. Viscosity is a strong function of salinity for high concentrations. Additionally, temperature can strongly affect viscosity, and the potentially different thermal environment of water on Mars from typical Earth ocean temperatures may represent another difference in their wave environments. Here too is the only dependence of the problem on liquid viscosity. So, as with air density, we believe that this term completely and correctly accounts for possible changes in the water viscosity on Paleo-Mars.

The next most significant term is the wave breaking term $S_{wb}$. This term (Donelan et al., 2012) is given by $S_{wb} = -42(1 + 120\mathrm{mss}(k,\phi))^2[k^4F(k,\phi)]^{2.5}\omega F(k,\phi)$, where $\mathrm{mss}(k)$ is the mean slope squared of all waves longer than $2\pi/k$. $S_{wb}$ has no direct dependence on any of the 7 parameters we expect to vary at Mars (air density, viscosity, gravity, liquid viscosity, density, surface tension, wind speed). Instead, it only involves functions of the wave slope, frequency and wavenumber. The changes to $S_{wb}$ from these parameters are already automatically handled by modifying the dispersion relation for Mars. Thus, we expect this term to carry over to Mars with no explicit modification.

The non-linear, wave–wave interaction term is treated as being proportional to the magnitude of the wave breaking term. But instead of removing wave energy from the spectrum, it merely redistributes it within the spectrum. The UMWM model redistributes this energy into wavenumber and azimuth bins within two bins of the bin under consideration. This matches the observations on Earth very effectively. Because its form is the same as the wave breaking term, we also expect that this term will have no explicit dependence on the 7 parameters varying between Mars and Earth.

The enhanced dissipation due to breakers in the surf zone, $S_{br}$ is taken to be of the form of $S_{wb}$ with the multiplier, $coth(kd) - 1$, to account for the increased dissipation in shoaling waves. Consequently, this too will transition from Earth to Mars unchanged.

The final term in the radiative transfer equation is the bottom friction term, which only becomes important as the waves move into shallow water. Bottom friction depends on wave orbital velocities near the bottom and the roughness characteristics of the sediments and not on any of the 7 parameters that are expected to vary between Earth and Mars. The reduced water depth merely changes the wavelength, phase and group velocities of the waves, enhancing their steepness, producing energy convergence and enhanced bottom velocities. So, once again, we expect no explicit dependence on the 7 parameters expected to vary between Mars and Earth. The modified dispersion relation accounts for all of the relevant changes.

*3.2.2. The SWAN model*

SWAN (Booij et al., 1999) is one of the so-called third generation wave models that started in late '80s and early '90s with the precursor WAM model (WAMDI-Group, 1988; Komen et al., 1994). The basic idea of this generation of models is to represent the evolution of a wave field only on the basis of physical principles. Third generation models represent the basic tool in use by most of the world's meteo-oceanographic centers.

While the basic equation is still the radiative transfer equation (1), the expression of the various source terms on its right side differs from UMWM. Wave generation by wind is described by the classical approach by Miles (1957, 1959, 1960), later improved by Janssen (1989). Basically, waves grow because of the input of momentum by the overlying wind, Janssen pointing out that the downward momentum flux must also imply a reduction of the wind speed. The non-linear interaction term represents the conservative exchanges of energy among the spectral components. This term, originally proposed by Hasselmann (1962), is the best known one among the various source terms. However, its exact evaluation far exceeds the practical possibility. Hence a simplified version, the so-called Discrete Interaction Approximation, has been devised (Hasselmann et al., 1985). A three component resonant interaction is also possible in shallow water (Eldeberky, 1996; Eldeberky et al., 1997). Wave breaking in deep water, commonly referred to as

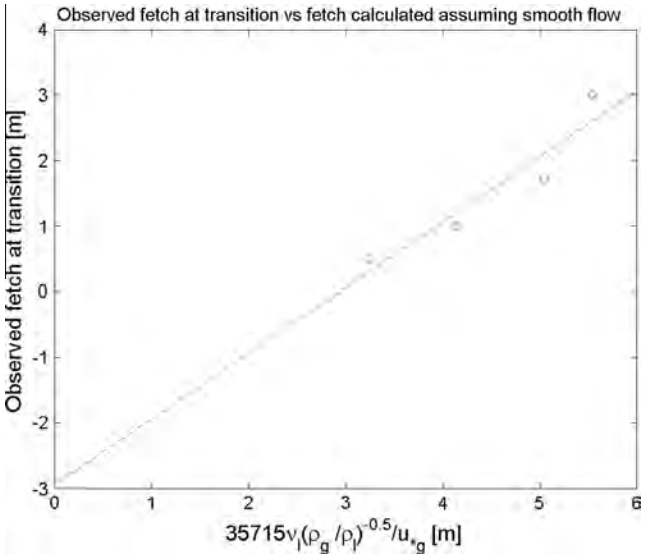


**Fig. 1.** Fetch at which transition to turbulent liquid flow was observed in a wave flume as a function of gas ($g$) and liquid ($l$) densities and gas friction velocity. Data are from Caulliez et al. (1996). These results justify the analytic expression for the transition to wave growth as a function of wind speed, liquid viscosity and the density ratio of the two fluids.

white-capping, is probably the least known part of the radiative transfer equation (1). Acting mostly on deep water conditions, we have used the empirical expression proposed by Komen et al. (1984). Approaching the shore and moving in progressively shallow water, waves begin to feel the bottom and become progressively steeper. Two processes become important at this stage: bottom friction dissipation and bottom induced breaking. For the former we have used the standard formulation by Madsen et al. (1989). For the latter we have followed the approach by Battjes and Janssen (1978), i.e. with the maximum ratio between wave height and local depth equal to 0.78, where this figure is also a function of the wavelength and of the shoaling bottom slope (see, e.g., Tsai et al., 2002).

Because SWAN is expressed in terms of the fundamental physics, we can simply apply the various parameters as may have existed on Mars in the past and run the model to predict the wave environment that should have existed under those conditions. With our application of SWAN (as with UMWM) there is no "tuning" of the model, only the proper recognition and replacement of the various parameters that would have been different on Paleo-Mars.

## 4. Model validation in the Mars wind tunnel

To validate the two wave models we use to predict the wave conditions that may have existed on ancient martian seas, we have directly compared their predictions with measurements in a wind tunnel that can be run at reduced pressures, approaching those of current Mars. By verifying the onset of wave generation, as well as the detailed wave spectrum that developed at higher winds, we have proven that our models are accurate under conditions far from the sea level terrestrial conditions for which they were originally developed and tested.

However, before we compare the models to the wind tunnel data, we need to more carefully examine the physics of the onset of wave formation. This is crucial because one of the doubts in the literature (e.g., Lorenz et al., 2005) was if winds at a highly reduced pressure could still trigger the onset of wave generation. There are two different conditions that must both be met for wave generation to occur. These will be different on Mars than on Earth, and must be accounted for to fully understand our small wind-tunnel wave-tank modeling. Section 4.1 discusses these processes and thus the changes to the onset of wave generation that would occur under different conditions from terrestrial. The details of the wind-tunnel wave-tank experiments are discussed in Section 4.2 and finally the data are compared against the models in Section 4.3.

### 4.1. Threshold wind speeds

Waves grow in response to a feedback process modeled using the mechanism of Miles (1957, 1959, 1960) in SWAN and that of Jeffreys (1924, 1925) in UMWM. Here we follow the limiting conditions as they appear in the UMWM model, but similar conditions apply to the SWAN model. In the UMWM model, waves appear to begin growing when the feedback mechanism (1st term of $S_{in}$ in (2)) exceeds the wave dissipation due to liquid viscosity (2nd term of $S_{in}$); i.e. $S_{in} > 0$. This threshold velocity has been suggested by Donelan and Pierson (1987) and demonstrated to be sensitive to water viscosity by Donelan and Plant (2009). It is largely dependent on liquid viscosity and is called the "$v_l$" threshold. This is the first condition that must be met for waves to be produced by wind on a flat surface, and will vary on ancient Mars due to changes in the gravitational acceleration, the fluid densities and the viscosity of the briny, possibly cold water differing from that of terrestrial sea water.

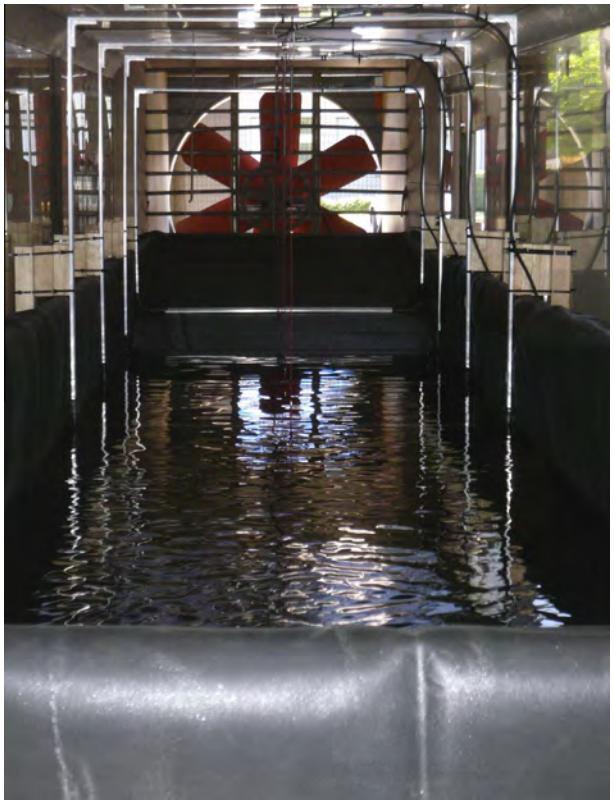

**Fig. 2.** Picture of the martian wave flume installed in the MARSWIT martian wind tunnel at NASA Ames. This shot is looking downwind along the axis of the wind tunnel. The fan used to generate winds near atmospheric pressure is seen at the end of the wind tunnel. The horizontal grates just upwind from that are injectors used to generate winds at low pressures. The 4 metal hoops are supports for the 4 wave staffs used to measure wave height in the experiment. The red sensor wires can be seen along the mid-line of the wind tunnel. The black bottom of the tank is a waterproof rubber membrane. The flume is not filled to operating levels in this picture and the most distant wave staff is completely out of the (low) water midway up the downwind 'beach'. (For interpretation of the references to color in this figure legend, the reader is referred to the web version of this article.)

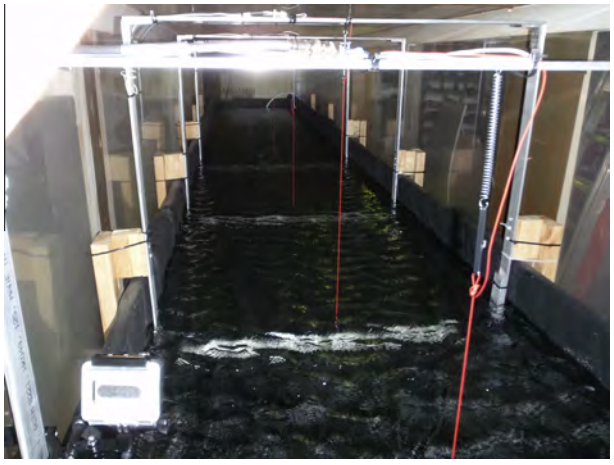

**Fig. 3.** Picture of the martian wave flume, in this case looking upwind from the downwind 'beach'. In this case, sea level pressure winds are blowing and waves are being generated. The red sensor wires of the wave staff are clearly seen in this image. The total fetch to the nearest sensor wire is 557 cm and to the second sensor wire is 480 cm. The water depth here is about 16 cm. (For interpretation of the references to color in this figure legend, the reader is referred to the web version of this article.)

The initial surface disturbance appears to be due to turbulent fluctuations beneath the surface (Caulliez et al., 1996, 1998), which change the growth with fetch from weakly exponential to strongly exponential ("explosive") at the point of transition to turbulence of the initially laminar liquid boundary layer. We identify that sudden increase in growth rate with the point at which the liquid turbulence induced wavelets (height, $h$) are large enough to penetrate the viscous gas boundary layer (depth, $\delta$) and interact directly with the turbulent gas flow (Donelan, 1990). This threshold wind speed for $h/\delta = 1$ provides a second constraint on the velocity and pressure fields for which there can be any wave growth at all. Because of the differences in gravity and air density at Mars, this criterion will also change from the standard terrestrial condition.

The thickness of the fully developed viscous gas sub-layer, $\delta$ is given by: $\delta = \frac{5\nu_g}{u_{*g}}$, where $u_{*g}$ is the friction velocity in the gas boundary layer and $\nu_g$ is the kinematic viscosity of the gas. The kinematic viscosity is inversely related to density (or pressure) – the dynamic viscosity being nearly independent of pressure. The height of the turbulence-induced roughness may be deduced from the vertical turbulent fluctuations acting against gravity: $h = \frac{\alpha u_{*l}^2}{g}$, where $u_{*l}$ is the friction velocity in the liquid, and $\alpha$ is a dimensionless constant that is determined by comparison with the observed thresholds from our low pressure wind tunnel experiments. Since there are no wind-generated waves at the transition, stress continuity across the surface can be assumed $(u_{*l} = u_{*g}\sqrt{\rho_g/\rho_l})$ and the threshold occurs at: $\frac{h}{\delta} = \frac{\alpha\rho_g u_{*g}^3}{5\rho g \nu_g} = 1$. This threshold is largely dependent on gas viscosity and is called the "$\nu_g$" threshold.

The conclusion is that, for given air and water conditions, for any wave generation the wind speed must be higher than the larger of the two considered thresholds. The point of transition to turbulence of the liquid flow may be several meters downwind (Caulliez et al., 1996). This transition therefore imposes a fetch dependent wind speed threshold below which the liquid boundary layer remains laminar and no waves are amplified by the wind. The rate of boundary layer development is proportional to the liquid friction velocity, $u_{*l}$ and inversely proportional to its viscosity, $\nu_l$. We have used the experimental results from Caulliez et al. (1996) to determine the wind speed, liquid viscosity and gas-to-liquid density ratio dependent fetch for the transition to wave amplification. The results from Caulliez et al. (1996) are plotted in Fig. 1 and demonstrate that the relation is well represented by: $x = \frac{35{,}715\nu_l}{u_{*g}\sqrt{\rho_g/\rho_l}} - 2.94$ m. For fetches shorter than this, no wave growth will occur. For fetches longer than this, wave growth will be found. At low pressure and low wind speed this fetch may well be larger than the length of a wind-wave tank. In particular, we demonstrate below that this is what occurred in the experiments reported by Lorenz et al. (2005).

### 4.2. Experimental setup

To test whether the wave models accurately represent the wave-forming capabilities of reduced density winds, we constructed a wave flume within the Mars boundary layer wind tunnel at NASA Ames. In this facility, we were able to control the atmospheric pressure and the winds blowing over a tank of water that we inserted within the wind tunnel. By sampling different combinations of atmospheric pressure and wind speed, we were able to explore the boundary between where waves can and cannot be generated by low-density winds (at least within the fetch limits in the wind tunnel). This did not allow us to explore varying gravity (difficult to do on Earth), nor did we attempt to modify the salinity or viscosity of the water in the tank. However, we believe that the single most important term that differs between current terrestrial oceanic conditions and those likely to be experienced on Paleo-Mars is the density of the atmosphere blowing over the open water.

**Table 1**
Experimental pressure and wind speeds and resulting wave heights.

| Pressure (mbar) | Wind speed @28.5 cm (m/s) | Significant wave height (mm) |
|---|---|---|
| 630 | 3 | 0 |
| 630 | 4 | 0 |
| 550 | 10 | 22 |
| 500 | 10 | 20 |
| 450 | 10 | 20 |
| 400 | 10 | 20 |
| 350 | 15 | 23 |
| 300 | 5 | 0 |
| 300 | 7 | 2 |
| 300 | 8 | 7 |
| 300 | 10 | 16 |
| 300 | 12 | 20 |
| 300 | 15 | 29 |
| 300 | 17.5 | 34 |
| 275 | 15 | 29 |
| 230 | 15 | 22 |
| 195 | 15 | 21 |
| 180 | 15 | 20 |
| 165 | 15 | 21 |
| 150 | 15 | 20 |
| 100 | 10 | 0 |
| 100 | 12.5 | 3 |
| 100 | 15 | 7 |
| 100 | 20 | 16 |
| 100 | 25 | 32 |
| 100 | 30 | 30 |
| 40 | 23 | 1 |
| 40 | 25 | 4 |
| 40 | 30 | 14 |
| 40 | 40 | 33 |

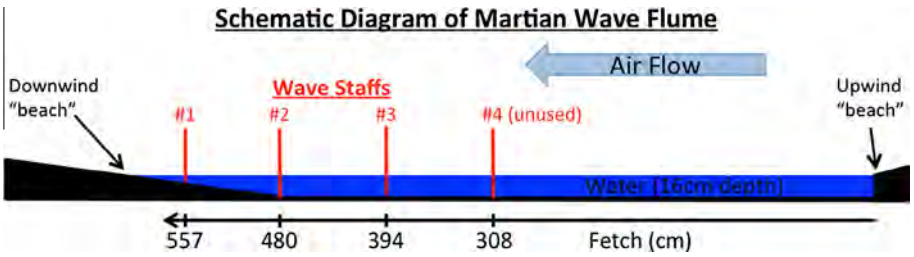


**Fig. 4.** Schematic diagram of the martian wave flume. In this diagram, the wind flows from right to left. A midline axial cross-section of the flume is indicated by the black shapes, showing the flume bottom, the upwind end and 'beach', and the downwind 'beach'. The water in the flume is shown in blue and has a nominal depth of 16 cm. The fetch of the wave flume is measured from the upwind end of the water, and extends about 6 m to the nominal location of the downwind 'beach'. The wave staffs to sense the time dependent wave height are located at the fetches indicated on the figure. The most valuable data was returned from wave staff #2 at 480 cm fetch. (For interpretation of the references to color in this figure legend, the reader is referred to the web version of this article.)

The NASA Ames MarsWIT facility is an open circuit wind tunnel with a cross section 1.2 m wide × 0.9 m high and a length of 13 m. It sits within a former Titan missile test chamber that can be evacuated to typical current martian pressures (roughly 6 mbar). Due to safety considerations, it can only operate with the gas being terrestrial atmosphere (air, not $CO_2$), but density scaling can be performed to account for the mean molecular mass difference between $CO_2$ and air. At pressures below about 600 mbar, the winds in the wind tunnel are created by controlled leaks into the chamber to create flow through the wind tunnel. Consequently, the winds that can be produced are a function of the ambient pressure, and the ambient pressure changes with time as the winds are produced. Typical winds that we could achieve were up to ~40 m/s at pressures below ~100 mbar dropping to about 15 m/s by the time the pressure reached ~600 mbar. At pressures above 600 mbar a fan driven system can provide the winds in the tunnel, but we only used the fan to check our system's performance under 1 bar conditions.

The wave tank was built to nearly fully occupy the width and length of the wind tunnel (see Figs. 2–4). The width was maximized to minimize edge effects in the tunnel, and the length maximized to allow the waves to grow as much as possible beyond the surface tension regime and into the gravity regime. Our initial estimates suggested that a wave tank with a fetch of ~6 m (the longest we could fit within the wind tunnel) would achieve this. The wave tank was 80 cm wide and had a total fetch of ~6 m long, and provided a water depth of about 16 cm (which we concluded was enough to effectively provide "deep water" for the waves likely to be generated in this limited fetch). We could not make the wave tank any longer than this ~6 m fetch, even though the wind tunnel

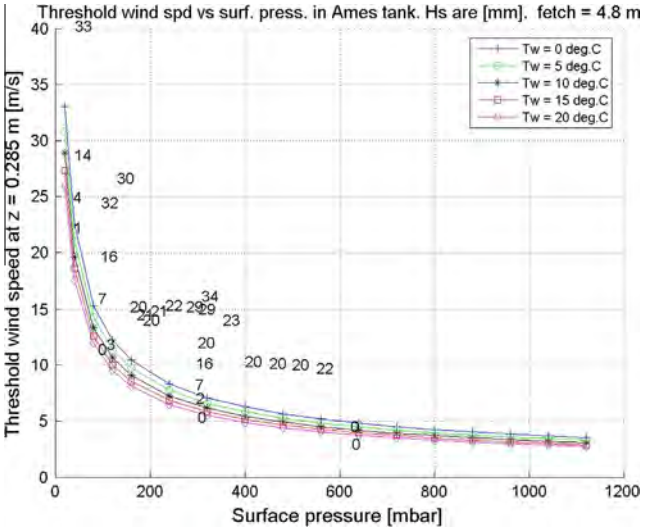


**Fig. 5.** This plot shows the significant wave heights (mm) that we measured in the martian wave flume under different atmospheric pressures (mbar) and wind speed (m/s) (see Table 1). The measurements are indicated with numbers for the wave heights in mm at the location in pressure and wind speed where they were obtained. The fetch for all the data is 4.8 m. The curves on the figure show the threshold below which no waves are expected to be generated for various choices of water temperature.

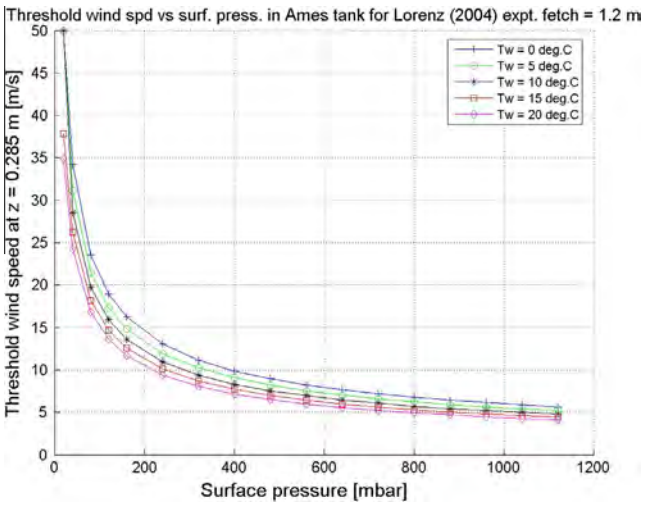


**Fig. 6.** As Fig. 5, but for a 1.2 m fetch. This figure is produced to allow comparison with the result in Lorenz et al. (2005) where a 1.2 m fetch wave tank was used in the MARSWIT wind tunnel. The lowest pressures they tested (300 mbar) generated no waves because the fetch available was too short for the wind speed and temperature of their tests. That does not mean that waves cannot be generated over long fetches for pressures of 300 mbar or lower.

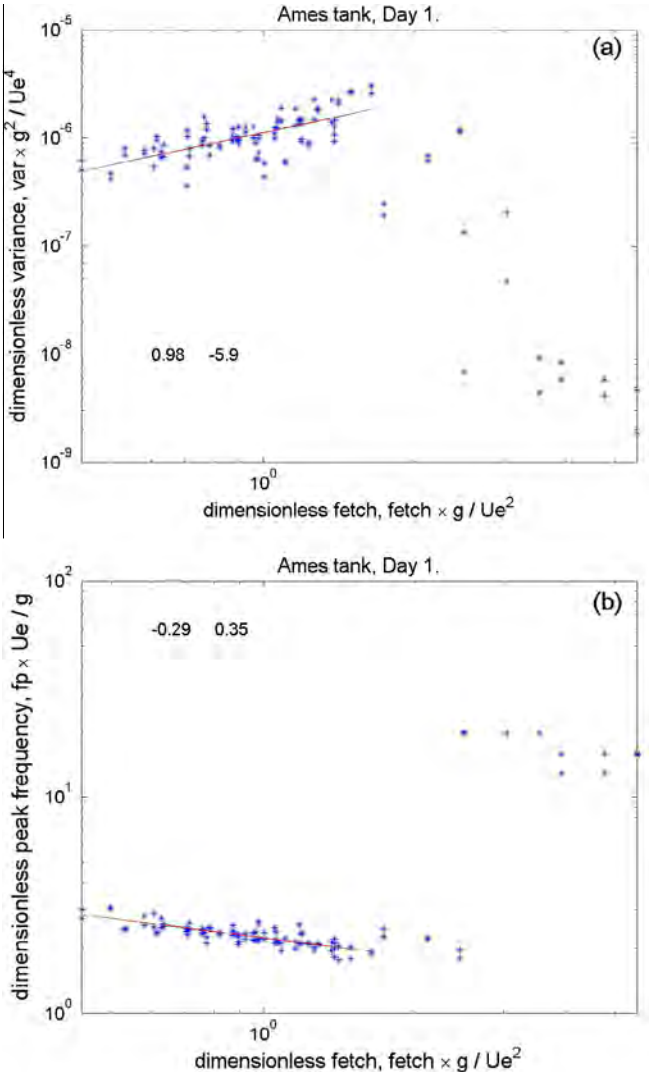


**Fig. 7.** (a) Dimensionless variance versus dimensionless fetch for the data recorded in the wave tank on Day 1 (June 15, 2010). (b) as in the upper panel, but for dimensionless peak frequency. The numbers on the figure are the slope and intercept (respectively) of the (red) regression line. (For interpretation of the references to color in this figure legend, the reader is referred to the web version of this article.)

itself is substantially longer than this. The pitot tubes to measure winds in the tunnel, and the leak injectors to create the winds limit the usable length to 6 m. At the upwind inlet of the wind tunnel, we constructed a smooth flare of the wind tunnel entrance to match the lip of the wave tank to avoid excessive turbulence at the start of the wave tank. The wave tank's upwind lip was slightly higher than the 16 cm depth of the water itself to avoid it spilling out of the wave tank. To avoid a discontinuity in the airflow there, we constructed a short ramp down to the water level. This also served as a small upwind "beach" to dissipate any waves that might reflect and propagate upwind. The downwind end of the wave tank was a much longer and shallower sloping region, to serve as a downwind beach to dissipate any waves at the end of the tank to avoid them reflecting and propagating upwind. This downwind beach started at the 16 cm depth of the tank and had a slope of 1:7, or in other words a length of about 210 cm to rise the ~30 cm from the bottom to the top of the wave tank. All of these design considerations for the wave tank were made not only to ensure that the low pressure waves we observed would be of measurable height (if they existed at all) and dominated by gravity as the restoring force, but also taking into consideration the extensive design experience that one of us (Donelan) has with wind-wave flumes.

We used capacitive wave staffs to measure the waves generated. These instruments have been used extensively in terrestrial wave measurement (both in the field and in wave flumes). They operate by measuring the effective capacitance of thin wires immersed vertically in the water. The wires are firmly held in position in the centerline of the wave tank and at various fetches downstream. As the waves move the water level up and down on the wires, the capacitance between the inner conductor of each wire and the water outside (with the insulation of the wire as the capacitor's dielectric) changes linearly with the surface elevation. We used custom electronics to measure the charging time of the thin-wire capacitor to a given voltage under a constant current. This charging time is then a proxy for the capacitance of the thin wire and can be measured with high accuracy and precision at a high repetition rate (100 Hz). These capacitances could then be translated to wave heights by recording the charging times while the wave tank was filled. In fact, we overfilled the tank (just before overflowing it) and used a linear regression on the measurements over the ~6 cm range of interest for each separate wave staff. The resulting precision on the wave height measurement was about 0.1 mm.

We had wave staffs located at fetches of 394 cm, 480 cm and 557 cm. These positions are indicated on the schematic in Fig. 4. The wave staff at 480 cm was just before the submerged toe of the downwind beach, and still had the full ~16 cm depth of the wave tank. The wave staff at 557 cm was about halfway up the beach, and only had about 6.3 cm of water depth at its location. While measurements at the longest fetch would seem to be the most valuable, the smaller depth at this site mid-way up the beach made it less reliable than the one at 480 cm for comparison with modeled waves, due to the growing importance of the bottom-related processes. The wave staff at 394 cm showed notably smaller wave heights than that at 480 cm as expected. An earlier study by Lorenz et al. (2005), which used a much smaller wave tank with fetches limited to 1.2 m, did not see any waves below a pressure of about 300 mbar with wind speeds up to 11 m/s. We demonstrate below that this was likely because of the fetch dependent threshold and the shorter fetches used in their study.

In addition to measuring the wave heights produced at these 3 different wave fetches, we also measured the water temperature in the tank. Evaporation, especially at the lowest atmospheric pressures tested, cooled the tank considerably. The physical properties of the fresh water we used in the tank did not vary tremendously over the ~10 °C temperature range we saw, but we were able to measure the temperature to account for these changes. However, the temperature sensor was not recorded on the first day at the wind tunnel, so the temperature then was estimated based on its behavior on subsequent days. The active tests were done on the 15th, 16th and 17th of June 2010, which we will call Day 1, 2 and 3.

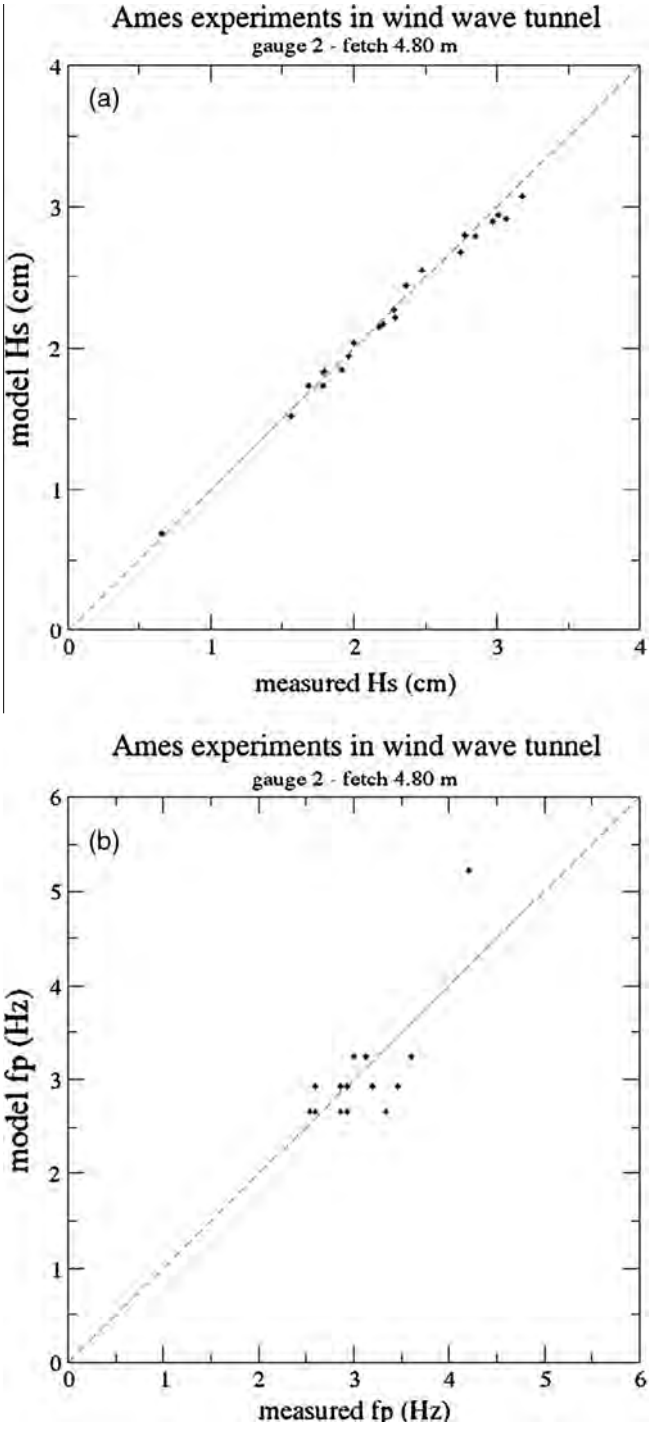


**Fig. 8.** Intercomparison between modeled and measured wave characteristics in the wave tank. (a) Significant wave heights, (b) peak frequency. This very good agreement between model and data suggest that the models accurately model the behavior even at reduced ambient pressures.

### 4.3. Experimental results

We conducted wave tests under pressures ranging from a low of 40 mbar to a high of 650 mbar (as well as at 1 bar) (see Table 1). The peak winds we could generate depended on the ambient pressure of each particular test, with the highest winds available at the lowest pressures. As discussed above, we could not easily control the pressure at all times. For a portion of the time, we could maintain the ambient pressure while producing wind via a controlled leak into the chamber because we could continue to evacuate the chamber to maintain the pressure. However, for the majority of the time, the pressure would systematically rise as we leaked air into the chamber to provide the wind. Consequently, we most often performed tests under a few different wind speeds as the pressure slowly crept upward. For each combination of pressure and wind, we would allow the wave tank to come to equilibrium with the wind over a period of 2 min, then we would sample the waves from each wave staff in turn for 45 s. We serially polled each wave staff because of interference between the timing circuits when multiple wave staffs were polled simultaneously. We believe this was due to ground loops in the bulk-head through to the pressure chamber of the wind tunnel. The 2 min settling time and the 45 s (per wave staff) sampling time was sufficient to produce consistent and well-documented results, especially in light of the need to minimize observation times in light of the slowly increasing pressure.

Our basic strategy was to identify the minimum wind that would produce detectable waves for a given pressure, and then to explore the behavior of the wave heights and spectra for wind speeds above that. In Fig. 5 significant heights [mm] for each run are plotted on pressure and wind speed axes. The data are from wave staff #2 at 4.8 m fetch. This figure not only shows the combinations of wind and pressure at which we took data, but also the wave heights that were realized at the 4.8 m fetch for each of those conditions (including wave heights of 0 mm). The curves also shown in Fig. 5 are the maxima of the three wave growth thresholds ($v_l$, $v_g$, $x$) for different water temperatures and $\alpha = 1200$. Water temperatures were between 4 °C and 9 °C and the observed thresholds fall on the curves. The choice of the dimensionless constant, $\alpha$ (Section 4.1), is thus determined and is transportable to different environments.

The expected thresholds for a fetch of 1.2 m (the tank length of Lorenz et al., 2005) are graphed in Fig. 6. The Lorenz et al. (2005) maximum wind speed of 11 m/s would not generate waves at 300 mbar and lower pressures with fetch limited to 1.2 m and water temperature less than 5 °C.

The development of gravity waves with fetch in a steady and uniform wind closely follows Kitaigorodskii's (1962) scaling laws with an approximately linear relationship between dimensionless variance (=variance $\times g^2/U_e^4$, where variance is the measured surface height variance) and dimensionless fetch (=fetch $\times g/U_e^2$) and an approximately $-1/3$ power law between dimensionless peak frequency ($=f_p \times U_e/g$, where $f_p$ is the peak frequency, see Appendix A) and dimensionless fetch (e.g. Hasselmann et al., 1973). Here we replace the measured wind speed, $U$ with an effective wind speed, $U_e$ to account for the reduced stress at low pressure: $U_e = U\sqrt{\rho_g/\rho_l}$. The dimensionless variance and peak frequency for Day 1 are graphed versus dimensionless fetch in Fig. 7. The data at short dimensionless fetch show (corresponding to strong effective winds) the characteristic behavior – indicated by the regression lines – with slopes of 0.98 and $-0.29$ as expected. However, beyond a dimensionless fetch of 1.65 – corresponding to light effective winds – the data fall/rise from the regression lines indicating the low variance/high frequencies associated with noise. These data mark the pressure dependent threshold and indicate that, beyond the threshold, the waves develop in much the same manner as they do in wind-wave tanks and in the field at normal atmospheric pressures.

The models (UMWM and SWAN) were exercised to compare with these above-threshold results. The aspect of the models relevant to this test is the wind input source function, $S_{in}$, which depends linearly on the ratio of densities ($\rho_g/\rho_l$). In the UMWM model the sheltering coefficient is increased from 0.11 (in the field) to 0.17 characteristic of the very short waves generated in tanks (see Donelan and Plant, 2009). SWAN was left unchanged. Both the models were run for all the cases considered in the wave tank (i.e. varying atmospheric pressure and wind speed). Both models recover the observed variances and peak frequencies quite well. Fig. 8 reports the respective comparison with the measured data from the SWAN simulations. Already obviously good, we point out that some of the scatter in the peak frequency diagram is to be attributed to the stepwise character of this variable and its large steps in the high frequency range consequent to the geometrical progression of the considered frequencies. Following these results, we are reassured that the models work in a wide range of pressures and wind speeds, and they are suitable for wave hindcasting on other planets with widely different atmospheres, oceans and gravity fields.

**Table 2**
Atmospheric characteristics considered for Paleo-Mars.

| Parameter | Units | Values tested |
|---|---|---|
| Pressure | mbar | 6, 60, 600, 1200 |
| Wind | m/s | 5, 10, 15, 20 |
| Temperature | °C | 0 |

**Table 3**
Ocean characteristics considered for Paleo-Mars.

| Parameter | Units | Ocean A | Ocean B | Ocean C |
|---|---|---|---|---|
| Density | kg/m$^3$ | 1010 | 1180 | 1360 |
| Viscosity | Pa s | 0.0018 | 0.0220 | 0.0420 |
| sfc.tension | N/m | 0.0722 | 0.0810 | 0.0900 |

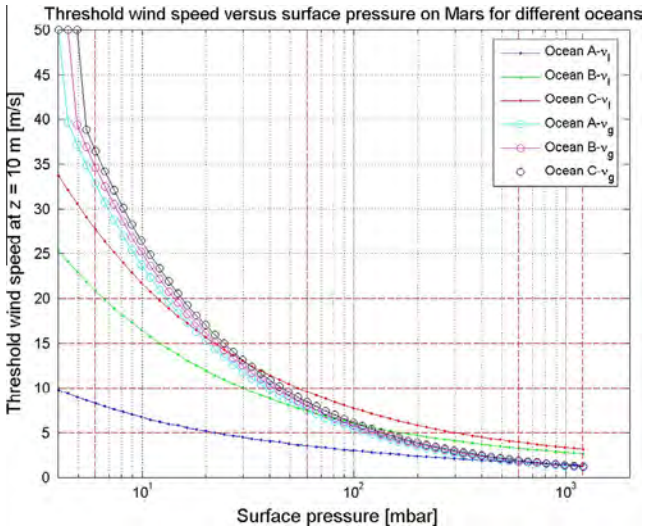


**Fig. 9.** Gas ($g$) and liquid ($l$) wind speed threshold for different atmospheric pressures on different oceanic conditions on Paleo-Mars (see Tables 2 and 3). For conditions below any of these curves (for a given Ocean), no waves would be expected to be produced, even for very long fetches. If wave-cut shorelines can be identified on Mars, this indicates that the atmospheric conditions (pressure and wind speed) were above the lines on this plot to ensure that wind-driven waves were produced.

## 5. The Mars environment

This section is devoted to estimating the wave conditions that, under a number of assumptions, could have been present on Mars in the past. Armed with the two validated wave models, we can now explore the possible wave conditions on Paleo-Mars. We begin by establishing the range of conditions to be explored with our modeling (atmospheric pressure, temperature, characteristics of the liquid that composed the martian seas) and the numerical and physical details of the experiments. This is done in Section 5.1. Given this information, in Section 5.2 we proceed to evaluate when waves were indeed possible and, if so, their characteristics as a function of fetch, depth, wind speed, pressure and oceanic conditions. The implications for the shore will be discussed in Section 6.

### 5.1. The atmospheric and oceanic conditions on Paleo-Mars

The wave conditions that may have existed on open bodies of water on early Mars depend on the size of the body of water (the fetch), as well as the atmospheric density, the water density and viscosity, and the wind speeds experienced. Unfortunately, there are no simple ways to accurately predict these parameters for early Mars. Indeed, a major motivation for studying this topic is to constrain the possible environmental conditions for early Mars. Nevertheless, we can make some assessments of the likely ranges of conditions that may have occurred on early Mars if there were open bodies of water. We will discuss these likely parameter ranges here and then use them to estimate the expected range of wave heights that may have once been found on Mars' seas.

The atmospheric pressure of early Mars is not well constrained by observations. There are geological signatures and more substantial recent evidence (e.g., Williams et al., 2013) that liquid water was once stable at the surface. This has been used by some to assert that the surface pressure on early Mars may have been as high as 500 mbar (or more), to allow a sufficiently strong greenhouse warming to raise the temperature enough for long-term water stability (e.g., Kasting, 1991; Mischna et al., 2000). Under various assumptions about cloud opacity and the freezing point depression of the ancient bodies of water on Mars, the pressure may have been significantly less than this as well. Thus, we will allow a very large range of possible early Mars atmospheric pressures, from the current 6 mbar up to slightly more than terrestrial, i.e., 1.2 bars. Specifically, we have modeled cases with surface pressures in a roughly geometric progression, i.e., 6, 60, 600, and 1200 mbar (see Table 2).

Wind speeds on early Mars have not been examined in detail, but we can expect that early Mars was similar to the current winds. Mischna et al. (2012) modeled the meridional temperature cross-sections of early Mars assuming a 500 mbar atmosphere, resulting in meridional gradients similar to those of current Mars. This suggests that zonal winds were similar in relative magnitude to those now found on Mars as well. Consequently, we used a range of wind speeds spanning those presently observed at the surface of Mars (e.g., Ryan et al., 1978). Specifically, we used winds of 5, 10, 15, and 20 m/s (see Table 2). However, in differing slightly with the measurements (which were typically taken at about 1.5 m elevation), we are assuming these wind speeds are relevant for 10 m elevation above the mean liquid level. Assuming a typical logarithmic wind profile, these wind speeds at 10 m elevation represent wind speeds about 2/3 as great at 1.5 m elevation, still consistent with current measured winds at the surface of Mars.

For temperature, we have assumed 0 °C for simplicity, although the actual liquid temperature could be well below that if the early martian seas were significantly briny. The temperature is a factor determining the atmospheric density (given the mean molecular mass, assuming a pure $CO_2$ atmosphere, and the atmospheric pressure), as well as the liquid's surface tension and viscosity. The changes in the atmospheric density between 0 °C and what might be a lower limit to a liquid (un-frozen) temperature even in extremely briny conditions (~240 K) only represent a 10% change in atmospheric density, so we will ignore that effect in light of the much larger uncertainties in the properties of early Mars. The behavior of the liquid's density does not change appreciably over this temperature range. Its surface tension and viscosity do change, but well within the uncertainties due to salinity differences. We will ignore the possibility that the surface temperature could be significantly different from 0 °C even with open seas on Mars,

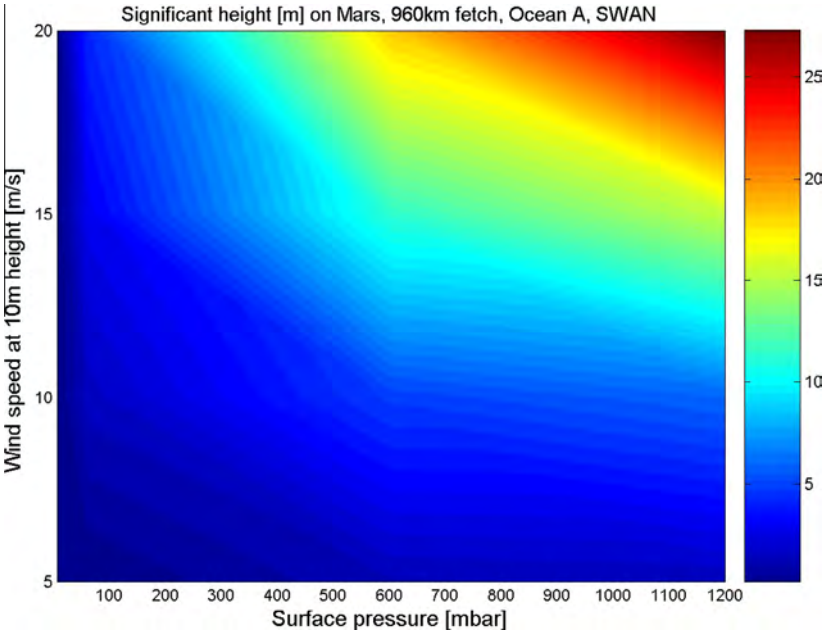


**Fig. 10.** Significant wave heights (m) on Mars Ocean A (see Table 3) for different wind speeds and surface pressures at 960 km of fetch. Results for SWAN wave model.

and assume it stays at 0 °C with little impact on the fidelity of our modeling.

For the martian sea-water, the principal effect in varying its parameters is the unknown salinity that it may have had. Recent observations by the MER rovers suggest that brines may have been frequent in early Mars. Tosca et al. (2011) estimated the properties of several different brines that may have been present on Mars. Many of these may have been extreme end-member brines and would not represent a full ocean's salinity, but in the absence of any more detailed information we will adopt them as the extreme cases for what Mars' seas may have been like. We chose to use three cases to test our modeling, signified as Ocean A, Ocean B and Ocean C with progressive increases in salinity. The lowest salinity case (Ocean A) was Tosca et al.'s Brine 1a. The highest salinity case (Ocean C) was Tosca et al.'s Brine 4b. Ocean B was chosen as the mean of these two extreme cases. The density, viscosity and surface tension for each of these three cases are indicated in Table 3, and were taken from Tosca et al. (2011). Combined with the four atmospheric pressures and four wind speeds, this leads to a total of 48 simulations. For each simulation we have used a constant and uniform wind speed. In these conditions the achievable wave heights are a function only of the dimension and geometry of the basin.

As basic reference we have considered a square basin with 1000 km sides. This is about half the size of Hellas in linear dimension and significantly smaller than the northern lowlands, but big-

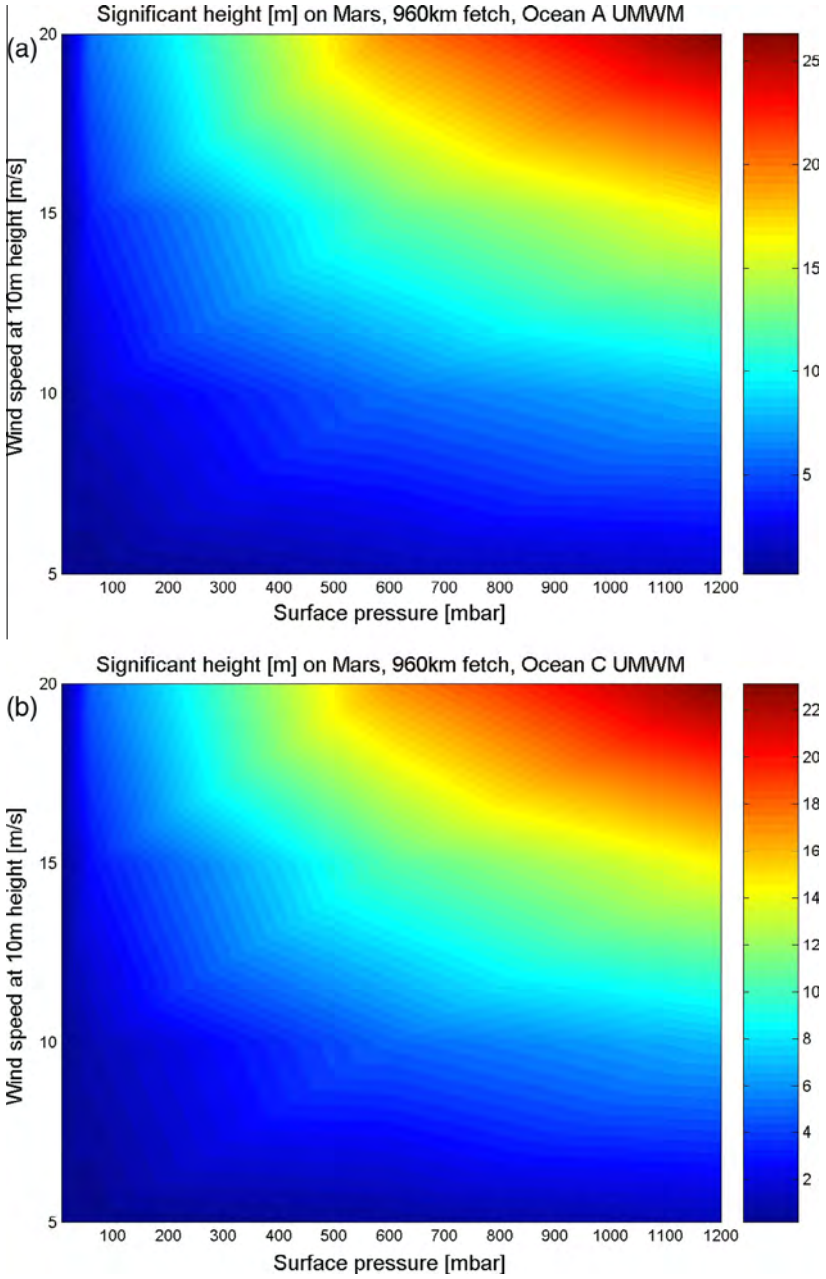


**Fig. 11.** Significant wave heights (m) on Mars for different wind speeds and surface pressures at 960 km of fetch modeled using the UMWM wave model. Panel (a) showed the results for Ocean A (see Table 3). This is nearly identical to Fig. 10, demonstrating that the two wave models produce essentially identical results (increasing our confidence in both). Panel (b) shows the results for Ocean C. These waves are ~10% smaller than those for Ocean A, mainly because of the difference in the liquid density between Ocean A and C.

ger than many of the smaller crater lakes that may have once existed on Mars. The wind is blowing perpendicular to one of the sides and, starting from flat calm conditions, we let the wind blow until equilibrium wave conditions are reached. Focusing our attention on the central axis of the basin, at the end of each run we have available full information about how wave characteristics, in particular wave height, and peak period vary with fetch, i.e. with the distance from the coast from which the wind blows. This provides information on the possible wave heights also for basins of smaller dimensions.

Deep water conditions (400 m) are assumed for the first 960 km. The largest waves we modeled were ~25 m high and 600 m long, so all of our waves would behave as deep-water waves in a 400 m deep model domain. A depth of 400 m is also likely quite conservative for any basin on Mars that approaches 1000 km on a side. On Mars, basins of this scale are measured in km of depth, rather than 100s of meters. After this the bottom progressively slopes up at 1% reaching the shore at the 1000 km line. The details of this slope are not important to the wave spectrum obtained before reaching this point (i.e., at 960 km fetch where we report our results). At all the grid points we have available full 2D spectral information from which all the relevant integrated wave parameters (significant wave height $H_s$, mean and peak period $T_m$, $T_p$, etc.) are derived. See Appendix A for their full definition.

### 5.2. Waves on Paleo-Mars

First we consider the conditions on Mars for which there will not be any wave growth. Both threshold wind speeds on Mars are graphed in Fig. 9 for the three oceans of Table 3. No waves at

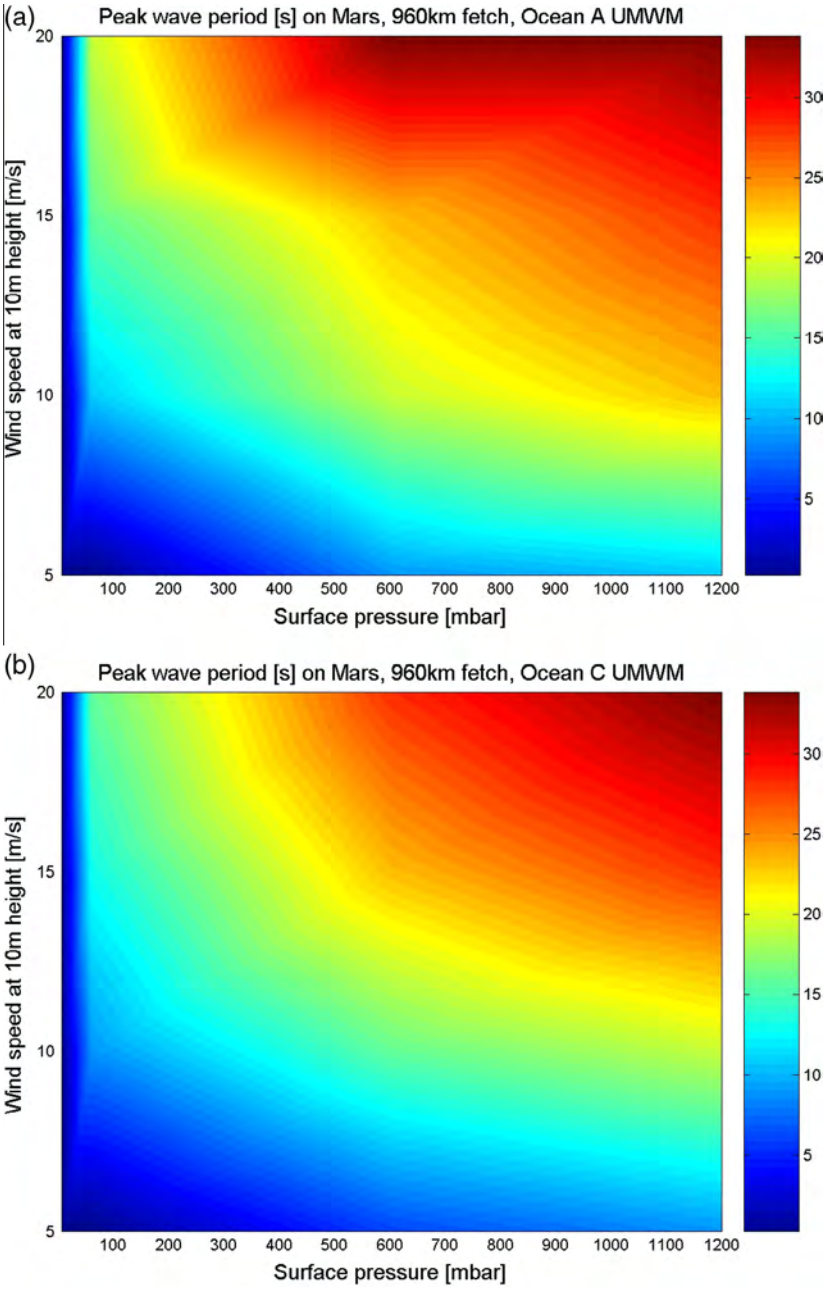


**Fig. 12.** As in Fig. 11, but for peak wave period.

wind speeds beneath the higher of the two curves ($v_g$, $v_l$) will grow at that pressure. Above 30 mbars the liquid viscosity threshold dominates for briny Ocean C, while at 800 mbars the liquid viscosity threshold dominates for the sea-water like Ocean A. Below 20 mbars the threshold is determined in all cases by gas viscosity. Waves will grow at wind speeds as low as 1.4 m/s at pressures of 1 bar on Ocean A. On the contrary no waves will grow at wind speeds beneath 13 m/s when the surface pressure is only 30 mbars. At 6 mbars (Mars' surface pressure today) it would take winds between 33 and 37 m/s to generate waves on Mars' putative oceans.

As mentioned above, we exercise the models (UMWM and SWAN) on a deep square ocean basin of side 1000 km. The threshold limits are applied to the model outputs, replacing them with zeros where conditions fall beneath the thresholds. The overall results for significant wave height $H_s$, for different pressures and wind speeds, and at 960 km fetch on Ocean A, are plotted for both the models, SWAN and UMWM, in Figs. 10 and 11a respectively. Before any quantitative comment on the results, we stress two points. First, the apparent discontinuities present in the plot isolines are due to the rather discrete values of the pressure and wind speed considered. Much more important, and relevant for our results, the quantitative similarity between the two plots strongly indicates that the models – tested on Earth against data – adjust in the same way to the changes in gravitational acceleration, pressure and viscosity. This strengthens our contention that the models do realistically simulate conditions on Mars and we can move with confidence to the analysis of the results. The similarity between the two model results holds for all the considered quantities. Therefore subsequent figures will be from one model or the other.

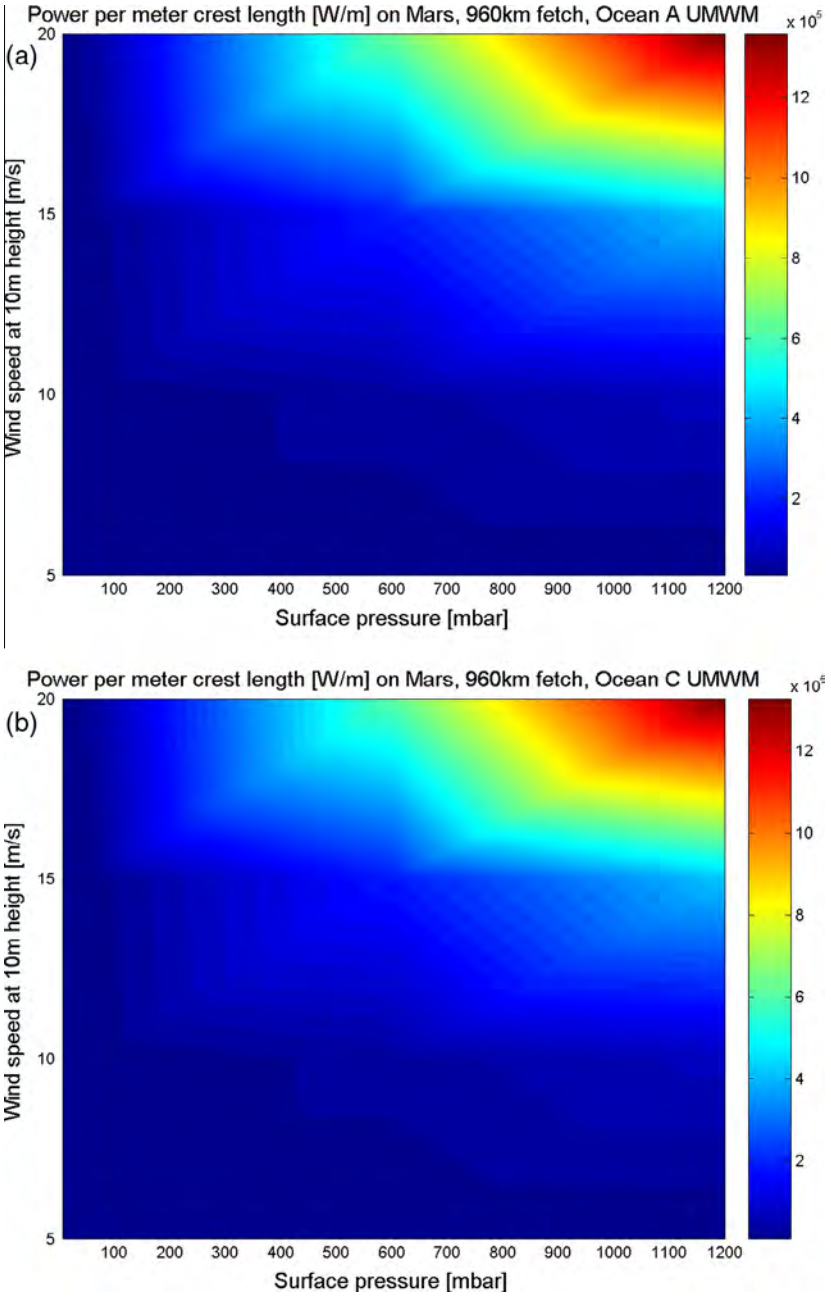


**Fig. 13.** As in Fig. 11, but for wave power flux per meter crest length (W/m).

To show the results, we return to Fig. 11a ($H_s$ for UMWM for Ocean A) and compare with the corresponding results for Ocean C (Fig. 11b). The distribution of significant wave heights, for the different pressures and wind speeds, is obviously similar in the two oceans. However, as seen from the color scales on the right of the plots, Ocean A hosts higher waves – see the peak values respectively at 24 and 22 m $H_s$. The reason (see Table 3) is the lower density of the liquid in Ocean A, the two differences being both of the order of (slightly larger than) 10%. Given that the energy input by wind is similar, this energy must lead to higher $H_s$ in the case of reduced liquid density. Note that we are reporting the results at 960 km fetch, i.e. still in deep water (400 m depth), before any shoaling towards the shore.

It is worthwhile to point out the differences from Earth. On our planet the maximum achievable significant wave height for a 20 m/s wind speed (and similar atmospheric pressures) is between 9 and 10 m. The lower value with respect to the ones in Fig. 11a (Ocean A, see Table 3) is mainly due to the different gravity on the two planets, hence the different phase speed of the waves (much larger on Earth), and hence the different energy input by wind (much larger on Mars).

We get a different perception of the wave characteristics on the two systems by looking at the peak periods $T_p$ in martian Oceans A and C, respectively in Fig. 12. First, note how the maximum $T_p$ values are similar in the two oceans, implying similar wavelengths. For $T_p$ = 30 s this corresponds to about 532 m wavelength. This is interesting in that the ratio $H_s/L_p$, with $L_p$ the peak period wavelength, for Ocean A is only slightly larger on Mars, 4.7%, with respect to the classical terrestrial value of 4%. This is likely related to the stronger wind forcing of the slower martian waves.

Relevant for the potential shoreline forming action on the coasts, in Fig. 13, we report the power flux at the 960 km fetch line, again for the considered pressures and wind speeds, and for Oceans A and C. The maximum 1.3 MW/m value holds for both the oceans. Given the similar phase and group speeds (as determined from Fig. 12), the similar power flux results from the lower wave heights in C associated with the higher density of the liquid brine.

Because Ocean B (see Table 1) has characteristics intermediate between Oceans A and C, it is not surprising that its wave characteristics lie between the two reported ones. This is clearly seen in Fig. 14 where we have plotted the power available in the three oceans for the different considered pressures and a 20 m/s wind speed. The different wave heights in the three systems are compensated for by the different liquid densities. The result is a practically equal power on all three oceans.

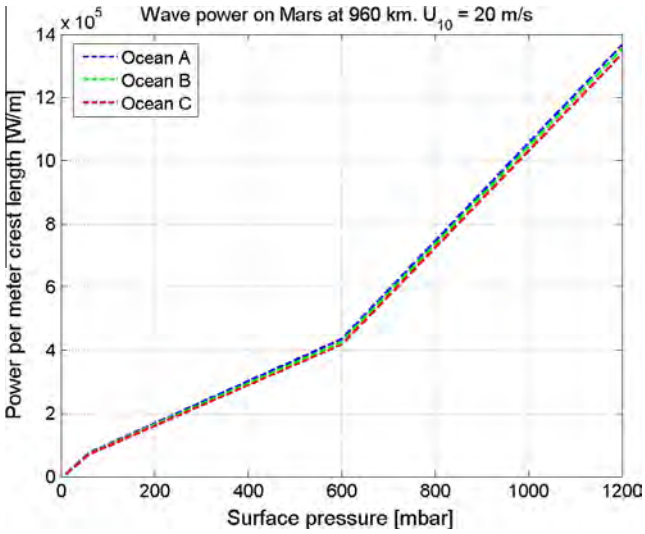


**Fig. 14.** Wave power per meter crest length (W/m) on Mars, at 960 km fetch, for different surface pressures and a 20 m/s wind speed. The almost overlapping curves are for the three Oceans A, B, C. See Table 3 for their characteristics. This demonstrates that salinity differences are only a small effect on the power in the wind-driven waves created.

## 6. The implications for Mars geological features

In this work, we have asked the question whether water waves could be created on open water on ancient Mars, under various possible atmospheric pressure conditions. We found that there are clear combinations of reasonable atmospheric pressure and wind where waves could be formed and other equally plausible combinations where waves could not be formed (i.e., see Fig. 9). In this sense, our work is valuable in that identifying wind-driven wave-cut shorelines on Mars can have some diagnostic capability for the atmospheric conditions that must have occurred at the time that extensive open water was present. We found that the other variables that could conceivably influence the wave environment on an ancient martian sea are much less important than wind speed and atmospheric pressure. The temperature and salinity of the sea would change its density, viscosity and surface tension, but these three effects would not present significant differences in the wave environment one would find, particularly when one considers the power deposited onto the shoreline by the various wave scenarios. Ultimately, it is this power deposition to the shoreline that creates the geomorphologic features that could be recognized some several billion years later to act as a record of the sea's existence. This means that the presence of a shoreline around an ancient martian sea is a good indicator of whether the pressure and wind speed was above all of the curves in Fig. 9.

We have not attempted to model the formation of a shoreline as was done in Kraal et al. (2006). In our opinion, the problem is too complex to adequately and definitively address. Kraal et al. (2006) addressed the question of whether benches could be cut into bedrock, finding that sea-level recession may not allow adequate time for benches to be cut. However, the duration over which a sea may have stood at a particular level at Mars is still unclear. We do not fully understand how water was delivered to this hypothetical sea (steadily or episodically or catastrophically) and so fully understanding its sea-level history is not yet possible. Smaller chains of lakes may have naturally regulated levels by overflowing their outlets, even in the presence of significant evaporation (e.g., Fassett and Head, 2008; Matsubara et al., 2011). With adequate fetch, these lakes may have had sufficient time to develop a shoreline under a variety of water delivery scenarios. Perhaps most importantly, it is unlikely that the only available material from which to form a recognizable beach would be bedrock. Williams et al. (2013) identified river-deposited material at the Curiosity rover site. The erosive action of the river flow identified by Curiosity is similar to the wave-induced bottom flow speeds of a shoaling wave. Fig. 15 shows the maximum bottom orbital velocity during the shoaling of the Ocean A waves seen in Fig. 10. Repetitive and long acting velocities of the order of 1 m/s or more would certainly be effective in sloping an unconsolidated shore. This wave formed beach could perhaps still be recognizable today.

The debate about the presence or absence of shorelines on seas or lakes at Mars is not concluded. Our work stands to help shape this debate whether or not shorelines are found, or whether some other approach can establish constraints on the ancient atmospheric pressure at Mars. In any case, our results can help narrow the permissible conditions that must have been obtained when open water may have existed on Mars. If wave-cut shorelines are eventually found, this will require that winds were above a given

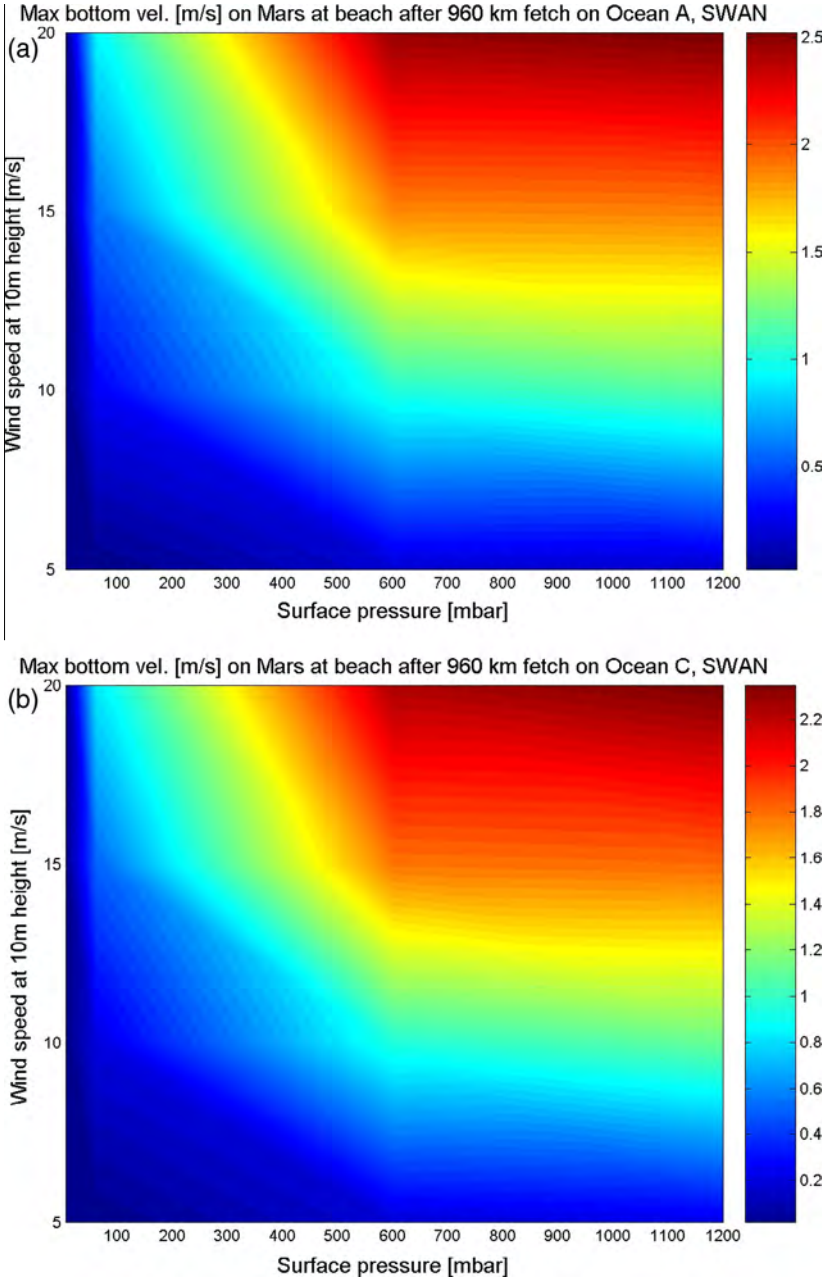


**Fig. 15.** Maximum bottom orbital velocity (m/s) during the shoaling of waves after 960 km fetch for different surface pressures (mbar) and wind speeds (m/s) using the SWAN model. Ocean A and C are considered. See Table 3 for their characteristics.

strength depending on the atmospheric pressure at the time (lower winds for higher pressures) as shown in Fig. 9.

## Acknowledgments

This research was partly supported by the Mars Fundamental Research Program. In particular, the wind tunnel experiments and the time for Don Banfield and Mark Donelan were supported by NASA Grant NNG07AV33G. Luigi Cavaleri has taken part to this project also under the Field-AC (FP7-SPACE-2009-1) and MyWave (SPA 2011.1.5 – 03) EU funded projects. The authors would like to acknowledge the invaluable assistance of Adam Saltzman in fabricating and executing the wind tunnel experiments, as well as J. Ken Smith and Tabb Prissel for their help at the wind tunnel.

## Appendix A

Definition of the integral quantities of a wave spectrum.

We consider the two-dimensional wave spectrum $F(f,\phi)$, with $f$ the frequency $(1-nf)$ and $\phi$ the direction $(1-n\phi)$ evaluated clock-wise with respect to geographic north. We define the following quantities:

Frequency spectrum $(\mathrm{m}^2\ \mathrm{s})$ $\quad E(f) = \sum_{1}^{n\phi} F(f,\phi)\cdot\Delta\phi$

Spectral moments $\quad m_n = \sum_{1}^{nf} E(f)\cdot f^n\cdot\Delta f$

Significant wave height $(\mathrm{m})$ $\quad H_s = 4\cdot\sqrt{m_0}$

Peak period (s) $T_p = 1/f_p$

with $f_p$ the frequency corresponding to the highest $E(f)$ value

Mean period (s) $T_m = \frac{m_0}{m_1}$

Mean direction $\phi_m = \tan^{-1}\left(\frac{\sum_1^{nf}\sum_1^{n\phi} F(f,\phi)\cdot\sin\phi\cdot\Delta\phi\cdot\Delta f}{\sum_1^{nf}\sum_1^{n\phi} F(f,\phi)\cdot\cos\phi\cdot\Delta\phi\cdot\Delta f}\right)$

## References


Battjes, J.A., Janssen, J.P.F.M., 1978. Energy loss and set-up due to breaking of random waves. In: Proc. 16th Int. Conf. Coastal Engineering, ASCE, New York, pp. 569–587.

Booij, N., Ris, R.C., Holthuijsen, L.H., 1999. A third-generation wave model for coastal regions. Part I. Model description and validation. J. Geophys. Res. C104, 7649–7666.

Carr, M., 1996. Water on Mars. Oxford University Press, New York.

Carr, M.H., Head III, J.W., 2003. Oceans on Mars: An assessment of the observational evidence and possible fate. J. Geophys. Res. 108 (E5). http://dx.doi.org/10.1029/2002JE001963.

Caulliez, G., Ricci, N., Dupont, R., 1996. On the coupling between the initial wind wave growth and the drift current structure. In: Donelan, M.A., Hui, W.H., Plant, W.J. (Eds.), The Air–Sea Interface. Rosenstiel School of Marine and Atmos. Science, University of Miami, Miami, pp. 27–34.

Caulliez, G., Ricci, N., Dupont, R., 1998. The generation of the first visible wind waves. Phys. Fluids 10, 757–759.

de Pablo, M.A., Pacifici, A., 2008. Geomorphological evidence of water level changes in Nepenthes Mensae, Mars. Icarus 196, 667–671.

Di Achille, G., Hynek, B.M., 2010. Ancient ocean on Mars supported by global distribution of deltas and valleys. Nat. Geosci. 3. http://dx.doi.org/10.1038/NGEO891.

Di Achille, G., Hynek, B.M., Searls, M.L., 2009. Positive identification of lake strandlines in Shalbatana Vallis. Mars. Geophys. Res. Lett. 36, L14201. http://dx.doi.org/10.1029/2009GL038854.

Di Achille, G., Ori, G.G., Reiss, D., 2007. Evidence for late Hesperian lacustrine activity in Shalbtana Vallis, Mars. J. Geophys. Res. 112, E07007. http://dx.doi.org/10.1029/2006JE002858.

Donelan, M.A., 1990. Air-sea interaction. In: LeMehaute, B., Hanes, D.M. (Eds.), The Sea. Ocean Engineering Science, vol. 9. John Wiley and Sons, pp. 239–292.

Donelan, M.A., Pierson, W.J., 1987. Radar scattering and equilibrium ranges in wind-generated waves – With application to scatterometry. J. Geophys. Res: Oceans 92 (C5), 4971–5029.

Donelan, M.A., Plant, W.J., 2009. A threshold for wind-wave growth. J. Geophys. Res. 114, C07012. http://dx.doi.org/10.1029/2008JC005238.

Donelan, M.A., Curcic, M., Chen, S.S., Magnusson, A.K., 2012. Modeling waves and wind stress. J. Geophys. Res. 117, C00J23. http://dx.doi.org/10.1029/2011JC007787.

Eldeberky, Y., 1996. Nonlinear Transformation of Spectra in Nearshore Zone. Ph.D. Thesis, Delft University of Technology, The Netherlands.

Eldeberky, Y., Sorensen, O.R., Battjes, J.A., 1997. Numerical simulation of wave transformation in the nearshore zone. In: Proc. Coastal Dynamics Conf., '97, ASCE, pp. 147–156.

Erkeling, G., Reiss, D., Heisinger, H., Poulet, F., Carter, J., Ivanov, M.A., Hauber, E., Jaumann, R., 2012. Valleys, paleolakes and possible shorelines at the Libya Montes/Isidis boundary: Implications for the hydrologic evolution of Mars. Icarus 219, 393–413.

Fairen, A.G., 2010. A cold and wet Mars. Icarus 208, 165–175.

Fassett, C.I., Head III, J.W., 2008. Valley network-fed, open-basin lakes on Mars: Distribution and implications for Noachian surface and subsurface hydrology. Icarus 198, 37–56.

Forbes, D.L., Taylor, R.B., 1994. Ice in the shore zone and the geomorphology of cold coasts. Prog. Phys. Geogr. 18, 59–89.

Ghatan, G.J., Zimbelman, J.R., 2006. Paucity of candidate coastal constructional landforms along proposed shorelines on Mars: Implications for a northern lowlands-filling ocean. Icarus 185, 171–196.

Grotzinger, J.P. et al., 2005. Stratigraphy, sedimentology and depositional environment of the Burns Formation, Meridiani Planum, Mars. Earth Planet. Sci. Lett. 240, 11–72.

Hasselmann, K., 1962. On the non-linear energy transfer in a gravity-wave spectrum, Part1: General theory. J. Fluid Mech. 12, 481–500.

Hasselmann, K. et al., 1973. Measurements of wind-wave growth and swell decay during the Joint North Sea Wave Project (JONSWAP)'. Ergnzungsheft zur Deutschen Hydrographischen Zeitschrift Reihe, A(8) (Nr. 12), 95pp.

Hasselmann, S., Hasselmann, K., Allender, J.H., Barnett, T.P., 1985. Computations and parameterizations of the nonlinear energy transfer in a gravity wave spectrum, Part 2: Parameterizations of the nonlinear energy transfer for application in wave models. J. Phys. Oceanogr. 15, 1378–1391.

Head III, J.W., Kreslavsky, M., Heisinger, H., Ivanov, M., Pratt, S., Seibert, N., 1998. Oceans in the past history of Mars: Tests for their presence using Mars Orbiter Laser Altimeter (MOLA) data. Geophys. Res. Lett. 25, 4401–4404.

Head III, J.W., Heisinger, H., Ivanov, M.A., Kreslavsky, M.A., Pratt, S., Thomson, B.J., 1999. Possible ancient oceans on Mars: Evidence from Mars Orbiter Laser Altimeter data. Science 286, 2134–2137.

Holthuijsen, L.H., 2007. Waves in Oceanic and Coastal Waters. Cambridge University Press, London, 404 pp.

Iijima, Y., Kazuhisa, G., Minoura, K., Komatsu, G., Imamura, F., 2014. Hydrodynamics of impact-induced tsunami over the Martian ocean. Plan. Sp. Sci. 95, 33–44.

Irwin III, R.P., Zimbelman, J.R., 2012. Morphometry of Great Basin pluvial shore landforms: Implications for paleolake basins on Mars. J. Geophys. Res. 117, E07004. http://dx.doi.org/10.1029/2012JE004046.

Ivanov, M.A., Head, J.W., 2001. Chryse Planitia, Mars: Topographic configuration, outflow channel continuity and sequence, and tests for hypothesized ancient bodies of water using Mars Orbiter Laser (MOLA) data. J. Geophys. Res. 106, 3275–3295.

Janssen, P.A.E.M., 1989. Wave-induced stress and the drag of air flow over sea waves. J. Phys. Oceanogr. 19, 745–754.

Jeffreys, H., 1924. On the formation of waves by wind. Proc. R. Soc. A 107, 189–206.

Jeffreys, H., 1925. On the formation of waves by wind, II. Proc. R. Soc. A 110, 341–347.

Kasting, J.F., 1991. $CO_2$ condensation and the climate of early Mars. Icarus 94, 1–13.

Kitaigorodskii, S.A., 1962. Applications of the theory of similarity to the analysis of wind-generated wave motion as a stochastic process. Bull. Acad. Sci. USSR Geophys. Ser. (1), 73–80.

Komen, G.J., Hasselmann, K., Hasselmann, S., 1984. On the existence of a fully developed windsea spectrum. J. Phys. Oceanogr. 14, 1271–1285.

Komen, G.J., Cavaleri, L., Donelan, M., Hasselmann, K., Hasselmann, S., Janssen, P.A.E.M., 1994. Dynamics and Modeling of Ocean Waves. Cambridge University Press, 560 pp.

Kraal, E.R., Asphaug, E., Moore, J.M., Lorenz, R.D., 2006. Quatitative geomorphic modeling of martian bedrock shorelines. J. Geophys. Res. 111, E03001. http://dx.doi.org/10.1029/2005JE002567, 13pp.

Leverington, D.W., Ghent, R.R., 2004. Differential subsidence and rebound in response to changes in water loading on Mars: Possible effects on the geometry of ancient shorelines. J. Geophys. Res. 109, E01005. http://dx.doi.org/10.1029/2003JE002141.

Lorenz, R.D., Kraal, E.R., Eddlemon, E.E., Cheney, J., Greeley, R., 2005. Sea-surface wave growth under extraterrestrial atmospheres: Preliminary wind tunnel experiments with applications to Mars and Titan. Icarus 175, 556–560.

Madsen, O.S., Poon, Y.-K., Graber, H.C., 1989. Spectral wave attenuation by bottom friction: Theory. In: Proc. 21st Conference Coastal Engineering, Malaga, ASCE, New York, pp. 492–504.

Malin, M.C., Edgett, K.S., 1999. Oceans or seas in the martian northern lowlands: High resolution imaging tests of proposed coastlines. Geophys. Res. Lett. 26, 3049–3052.

Matsubara, Y., Howard, A.D., Drummond, S.A., 2011. Hydrology of early Mars: Lake basins. J. Geophys. Res. 116, E04001. http://dx.doi.org/10.1029/2010JE003739.

Miles, J.W., 1957. On the generation of surface waves by shear flows. J. Fluid Mech. 3, 185–204.

Miles, J.W., 1959. On the generation of surface waves by shear flows. Part 2. J. Fluid Mech. 6, 568–582.

Miles, J.W., 1960. On the generation of surface waves by turbulent shear flows. J. Fluid Mech. 7, 469–478.

Mischna, M.A., Kasting, J.F., Pavlov, A., Freedman, R., 2000. Influence of carbon dioxide clouds on early martian climate. Icarus 145, 546–554.

Mischna, M.A., Lee, C., Richardson, M., 2012. Development of a fast accurate radiative transfer model for the martian atmosphere, past and present. J. Geophys. Res. 117, E10009. http://dx.doi.org/10.1029/2012JE004110.

Parker, T.J., Saunders, R.S., Schneeberger, D.M., 1989. Transitional morphology in the west Deuteronilus Mensae region of Mars: Implications for modification of the upland/lowland boundary. Icarus 82, 111–145.

Parker, T.J., Gorline, D.S., Saunders, R.S., Pieri, D., Schneeburger, D., 1993. Coastal geomorphology of the martian northern plains. J. Geophys. Res. 98, 11061–11078.

Perron, J.T., Mitrovica, J.X., Manga, M., Matsuyama, I., Richards, M.A., 2007. Evidence for an ancient martian ocean in the topography of deformed shorelines. Nature 447, 840–843.

Ryan, J.A., Henry, R.M., Hess, S.L., Leovy, C.B., Tillman, J.E., Walcek, C., 1978. Mars meteorology: Three seasons at the surface. Geophys. Res. Lett. 5, 715–718.

Squyres, S.W. et al., 2004. In situ evidence for an ancient aqueous environment at Meridiani Planum, Mars. Science 306, 1709–1714.

Tosca, N.J., McLennan, S.M., Lamb, M.P., Grotzinger, J.P., 2011. Physicochemical properties of concentrated martian surface waters. J. Geophys. Res. 116, E05004. http://dx.doi.org/10.1029/2010JE003700.

Tsai, C.-P., Chen, H.-B., Huang, M.-J., 2002. In: The Twelfth International Offshore and Polar Engineering Conference, Kitakyushu, Japan, May 26–31, 2002.

WAMDI-Group, 1988. The WAM model – A third generation ocean wave prediction model. J. Phys. Oceanogr. 18, 1775–1810.

Webb, V.E., 2004. Putative shorelines in northern Arabia Terra, Mars. J. Geophys. Res. 109, E09010. http://dx.doi.org/10.1029/2003JE002205.

Williams, R.M.E. et al., 2013. Martian fluvial congolomerates at Gale crater. Science 340, 1068–1072.